Visualizing the Stability of Critical Points in Uncertain Scalar Fields

Mihaela Mihai[a,*], Rüdiger Westermann[a]

[a] *Computer Graphics and Visualization Group, Technische Universität München, Germany*

Abstract

In scalar fields, critical points (points with vanishing derivatives) are important indicators of the topology of iso-contours. When the data values are affected by uncertainty, the locations and types of critical points vary and can no longer be predicted accurately. In this paper, we derive, from a given uncertain scalar ensemble, measures for the likelihood of the occurrence of critical points, with respect to both the positions and types of the critical points. In an ensemble, every instance is a possible occurrence of the phenomenon represented by the scalar values. We show that, by deriving confidence intervals for the gradient and the determinant and trace of the Hessian matrix in scalar ensembles, domain points can be classified according to whether a critical point can occur at a certain location and a specific type of critical point should be expected there. When the data uncertainty can be described stochastically via Gaussian distributed random variables, we show that even probabilistic measures for these events can be deduced.

Keywords: uncertainty, critical points, stability, scalar topology

1. Introduction

Scalar ensembles consist of several scalar fields, where every field or instance indicates a possible occurrence of the phenomenon represented by the data values. Ensembles are often generated numerically via multiple simulation runs with slightly perturbed input parameter settings. The rationale stems from the observation that the result of every run is affected by a certain degree of uncertainty, for instance, due to model simplifications or approximations inherent to the numerical schemes employed. Generating multiple instances helps predict and quantify the range of outcomes and, thus, allows us to classify features with respect to their stability across instances.

An important class of features in scalar fields is based on level-sets or iso-contours, i.e., the set of all points in the domain where the scalar field takes on a prescribed value, also called an iso-value. The effect of uncertainty on level-sets has been treated in several works [1], [2], or [3], which investigate the positional variations of level-sets due to uncertainty. Such an analysis, however, does not allow making reliable estimates of the possible geometric or topological variations of level-sets.

Recently, Pfaffelmoser et al. [4] have looked into the effect of uncertainty on the variability of gradients in scalar fields. Indicators for the likelihood of geometric changes of level-sets were derived from confidence intervals of the gradient magnitude and orientation, resulting in a stability analysis of both the shape and the slope of level-sets. By using a similar technique to propagate uncertainty for derived quantities in scalar fields that are linear combinations of the input values, and by introducing a method for non-linear combinations, we propose techniques to classify critical points in scalar ensemble fields with respect to different notions of stability. Interesting features often relate to critical points, since these indicate prominent surface components and their topological changes. Depending on the position and type of the critical points, the spatial locations where changes in the surface topology take place and the nature of these changes can be identified: Surface components emerge or vanish at minima and maxima, join or split at saddles.

Contribution: We investigate the associated gradient and Hessian matrix fields of the scalar ensemble members to identify the possible locations of the critical points, and assess their stability in type throughout the ensemble. We first summarize ensembles statistically and derive corresponding moments for the gradients. Since critical points occur where the gradients vanish, we use confidence intervals of the gradients to obtain quantities indicating the possibility of a critical point occurring around a given location. We then derive statistical summaries for the trace and determinant of the Hessian matrix, to give insight into the tendency of critical points to behave like minima, maxima, or saddles near a specified location in the ensemble.

The remainder of the paper is as follows: In the next section we review related work. We then introduce methods to analyze critical points in Section 3, which we visualize in Section 4. The proposed approaches are validated in Section 5 and demonstrated on two synthetic and two real world data sets in Section 6. We conclude the paper with a summary of the contributions.

2. Related Work

Uncertainty is a topic relevant to many research domains, and has been classified among the top research areas in visualization. Overviews of uncertainty visualization approaches are given, for instance, in Griethe and Schumann [5], Thomson et al. [6], or Potter et al. [7].

*Corresponding author.

Email addresses: mihaela.mihai@tum.de (Mihaela Mihai), westermann@tum.de (Rüdiger Westermann)

Uncertainty information has often been summarized by quantities such as mean and standard deviation, which have been encoded together with the actual data by means of color maps, opacity, texture, animation, glyphs, etc., in, for example Wittenbrink et al. [8], Djurcilov et al. [9], Rhodes et al. [10], Lundstrom et al. [11], and Sanyal et al. [12]. Although such methods indicate the amount of uncertainty affecting the data, they do not allow drawing conclusions on the way uncertainty affects specific features of the data, such as level-sets.

Several approaches have been proposed to visualize the effect of uncertainty on the position and structure of such features: Pang et al. [13] and Zehner et al.[14] use confidence envelopes containing an isosurface with a certain confidence, Grigoryan and Rheingans [15] displace each point on a surface along its surface normal to an extent proportional to the local uncertainty, while Brown [16] uses surface animation to illustrate the uncertainty of the values within different areas of the surface. Pfaffelmoser et al. [1] examine the positional and geometrical variation of level-sets, whereas Pfaffelmoser and Westermann [17], [18] incorporate correlation to offer insight into possible structural variations. Pöthkow and Hege [2] use the concept of numerical condition - the sensitivity of the output of a function to perturbations of the input data - to extract features in uncertain scalar fields, and apply it to visualize the positional uncertainty of level-sets. The proposed method was extended to include spatial correlation in Pöthkow et al. [19].

Further approaches to gain insight into salient features and their structure are based on topology. Overviews of methods dealing with topological features for both static and dynamic scalar fields, and especially for steady and time-dependent vector fields, are given in Theisel et al. [20], Laramee et al. [21], and Scheuermann and Tricoche [22]. For ensembles of uncertain scalar fields, Thompson et al. [23] introduce hixels - per sample histograms of values - to approximate topological structures of down-sampled data. Then, Wu and Zhang [3] enhance contour trees to represent uncertainty in the data values of the scalar fields and the position of the contours, as well as the variability of the contour trees themselves.

For uncertain vector fields, Otto et al. [24] generalize the concepts of stream lines and critical points to uncertain (Gaussian) vector field topology, in order to segment the topology by integrating particle density functions. Probabilistic local features, such as critical points, are extracted from Gaussian distributed vector fields using Monte Carlo sampling in Petz et al. [25], where the mathematical model for uncertainty considers the effect of spatial correlations. The method was extended to several types of non-parametric models for uncertainty in Pöthkow and Hege [26]. A fuzzy topology is proposed in Bhatia et al. [27], where the topological decomposition is performed by growing streamwaves, based on a representation for vector fields called edge maps. In the context of tractography, Schultz et al. [28] interpret critical points and other topological concepts based on probabilistic fiber tracking.

Numerous techniques have been introduced to assess different types of variations that uncertainty induces on level-sets and other such data features. To the best of our knowledge, however, no methods have been proposed to analyze and visualize the possible variations of critical points that are caused by uncertainty. Investigating different aspects of the stability of critical points and how uncertainty affects them would be beneficial, since critical points are indicative of prominent features and their topological changes, and such an analysis could serve as a starting point for further insight into the effects of uncertainty on level-sets and other related features.

While such studies have not been performed for uncertain data sets, critical points have been classified before according to different measures of stability and importance, for various purposes. For scalar fields, Edelsbrunner et al. [29] introduce the notion of homological persistence to assign importance measures to critical points and use it for topology simplification. Dey and Wenger [30] extend this notion to interval persistence, to assess which critical points are stable under perturbations of the scalar fields. Reininghaus et al. [31] use the persistence at multiple scales in scale space, to distinguish between minima and maxima with hill-, ridge-, or outlier-like spatial extent.

Topological persistence is used in the context of MS complexes, which decompose manifolds into regions of uniform gradient flow behavior to investigate the topology of the surfaces. Segmenting the surface into cells of uniform flow helps identify its various features and the way they are connected. Critical points, connected by lines of steepest descent, are the nodes of the MS complex. Successively eliminating critical points with an importance measure under a certain threshold results in a hierarchy of MS complexes. e.g., Bremer et al. [32] or Edelsbrunner et al. [33]. The methods require nonetheless a series of assumptions, as well as numerical integration. For these reasons and because we are interested exclusively in stability aspects of the critical points themselves, we do not compute MS complexes, even though we also use the gradient vector fields and Hessian matrices in our analysis.

For vector fields, various measures have been used to classify the importance of critical points, such as the Euclidean distance between critical points in Tricoche et al. [34] or the area of their corresponding flow regions in the topology graph in De Leeuw and Van Liere [35]. Wang et al. [36] use the topological notion of robustness to quantify the stability of critical points with respect to perturbations for stationary and time-varying vector fields.

3. Critical Points in Ensembles

Critical points of scalar fields are those points where the gradient vector vanishes. Several methods can be applied to locate critical points in scalar data sets: finding the crossings of the zero-contours of the x- and y-components of the gradient vector field, or the grid points with non-zero Poincaré indices, etc. The locations of critical points, however, are affected by the uncertainty in the data, which causes variations in the positions and types of critical points throughout the ensemble. We are therefore interested to indicate how likely it is that a critical point occurs around a given location and, if so, whether a certain kind of behavior should be expected there. In the following, we use two notions of stability: *Positional stability* refers to locations around which critical points occur repeatedly in the ensemble members, while *type stability* is used to characterize the positions near which critical points of the same nature emerge consistently throughout the ensemble.

To this purpose we do not use the actual critical points of the individual ensemble members. Instead, we derive two types of indicator functions at every vertex of a Cartesian grid and show the chances of a critical point of a certain type occurring close to the vertices, i.e., the stability in position and type. As gradients and Hessian matrices are fundamental to finding critical points and their types, we summarize these quantities statistically via confidence intervals and use them to derive the indicators.

3.1. *Confidence Intervals*

For scalar data sets given at the vertices of a 2D Cartesian grid structure, the data uncertainty is modeled by a multivariate random variable X, with components $X_{i,j}$ at each grid point $x_{i,j}$. We express the range of possible data values at each vertex using intervals, $[\mu(X_{i,j}) - \sigma(X_{i,j}), \mu(X_{i,j}) + \sigma(X_{i,j})]$, where $\mu(X_{i,j})$ is the mean value and $\sigma(X_{i,j})$ the standard deviation - a measure of the data variability at the grid point. For specific probability distributions of the random variables, confidence intervals of various confidence levels can be constructed. The aforementioned interval corresponds to a 68% confidence level for a 1D Gaussian distributed variable, i.e., there is a 68% probability that the true value lies in the confidence interval. In the following, we call $[\mu(X_{i,j}) - \sigma(X_{i,j}), \mu(X_{i,j}) + \sigma(X_{i,j})]$ a confidence interval irrespective of the probability distribution, although we assign confidence levels only for Gaussian distributions.

The uncertainty in the data also affects the variability of derived quantities that depend on the values at neighboring grid points, such as partial derivatives. To quantify the latter, we express the derived quantities in terms of functions of the random variables at neighboring vertices, and propagate the uncertainty from the input variables to the outputs. We thus obtain confidence intervals for the derived quantities. The exact procedure depends on the function relating the input to the output.

Propagating the uncertainty for first-order partial derivatives, where the functions approximating the output quantities are linear combinations of the values at the neighboring points of a grid vertex, has been treated before by Pfaffelmoser et. al [4]. The paper assesses the variability of gradients in 2D uncertain scalar fields and derives confidence intervals for the gradient magnitude and orientation. We follow their approach to obtain confidence regions for quantities that can be modeled using linear combinations of the input variables, such as the gradient, the Hessian matrix, and the trace of the Hessian matrix. For non-linear combinations, such as the determinant of the Hessian matrix, we propagate the uncertainty by linearizing the function by a first-order Taylor approximation.

3.2. *Confidence Intervals for Gradients*

To propagate the uncertainty for the gradient, we first approximate the gradient $\nabla X_{i,j}$ using the central differences kernel A_∇ on a stencil $s_1(X_{i,j})$ holding the four random variables at the non-diagonal neighbors of the vertex (cf. Figure 1),

$$\nabla X_{i,j} = A_\nabla s_1(X_{i,j}). \tag{1}$$

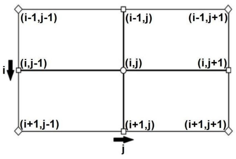

$$s_1(X_{i,j}) = [X_{i-1,j}, X_{i+1,j}, X_{i,j-1}, X_{i,j+1}]$$
$$s_2(X_{i,j}) = [s_1(X_{i,j}), X_{i-1,j-1}, X_{i-1,j+1}, X_{i+1,j-1}, X_{i+1,j+1}]$$
$$s_3(X_{i,j}) = [X_{xx}, X_{yy}, X_{xy}]$$

Figure 1: Stencils of random variables used in approximations.

The linear operator A_∇ can then be applied to obtain a mean $\mu_\nabla(X_{i,j})$ and covariance matrix $\Sigma_\nabla(X_{i,j})$ at every grid point

$$\mu_\nabla(X_{i,j}) = A_\nabla \mu(s_1(X_{i,j})), \tag{2}$$
$$\Sigma_\nabla(X_{i,j}) = A_\nabla \Sigma(s_1(X_{i,j})) A_\nabla^{\mathrm{T}}. \tag{3}$$

The input variables are $\mu(s_1(X_{i,j}))$, a four-element vector comprising the mean values $\mu(s_1(X_{i,j})_k)$ at each element of the stencil, and $\Sigma(s_1(X_{i,j}))$, a 4x4 covariance matrix, with the squared standard deviations $\sigma(s_1(X_{i,j})_k)^2$ as diagonal elements, and the covariances $\sigma(s_1(X_{i,j})_k)\sigma(s_1(X_{i,j})_l)\rho(s_1(X_{i,j})_k, s_1(X_{i,j})_l)$ of each pair of elements of the stencil as non-diagonal elements. The non-diagonal elements consider the correlations between neighboring random variables $\rho\left(s_1(X_{i,j})_k, s_1(X_{i,j})_l\right)$. The output variables are the gradient mean $\mu_\nabla(x_{i,j})$, consisting of the mean values of the first-order partial derivatives in the x- and y-directions, and the covariance matrix $\Sigma_\nabla(x_{i,j})$ of dimension 2x2, holding the squared standard deviations and the covariances of the first-order partial derivatives.

Note that, while standard deviations are sufficient to indicate the uncertainty in the scalar data, a 2x2 covariance matrix is now necessary to express the variability in the two directions of the gradient, as well as their correlation. Consequently, instead of two confidence intervals for each of the two directions, we derive a confidence region corresponding to the covariance matrix $\mu_\nabla(X_{i,j})^{\mathrm{T}} \Sigma_\nabla(X_{i,j})^{-1} \mu_\nabla(X_{i,j}) \leq 1$.

3.3. *Confidence Intervals for the Hessian Matrix*

Derivations are similar for the second-order derivatives, except that the central differences kernel A_H is now applied on a nine-point stencil $s_2(x_{i,j})$, holding the point itself and all of its neighbors (cf. Figure 1). Uncertainty is propagated for the Hessian matrix according to the following equations

$$\mu_H(X_{i,j}) = A_H \mu(s_2(X_{i,j})), \tag{4}$$
$$\Sigma_H(X_{i,j}) = A_H \Sigma(s_2(X_{i,j})) A_H^{\mathrm{T}}. \tag{5}$$

The output variables are $\mu_H(X_{i,j})$, a three-element vector holding the mean values of the second-order partial derivatives, and $\Sigma_H(X_{i,j})$, the covariance matrix of dimension 3x3. We do not use these uncertainty parameters to derive a confidence region, but regard them as inputs to other scalar output quantities, the trace and the determinant of the Hessian matrix.

For the trace of the Hessian, $\mathrm{tr}(H) = X_{xx} + X_{yy}$, the equations

$$\mu_{\mathrm{tr}}(X_{i,j}) = A_{\mathrm{tr}} \mu(s_3(X_{i,j})), \tag{6}$$
$$\sigma_{\mathrm{tr}}(X_{i,j}) = \sqrt{A_{\mathrm{tr}} \Sigma(s_3(X_{i,j})) A_{\mathrm{tr}}^{\mathrm{T}}}, \tag{7}$$

yield a mean $\mu_{\text{tr}}(X_{i,j})$ and a standard deviation $\sigma_{\text{tr}}(X_{i,j})$ at every grid vertex. The linear operator $A_{\text{tr}} = [1, 1, 0]$ is applied on the three-element stencil $s_3(X_{i,j})$ holding the second-order derivatives, to obtain $[\mu_{\text{tr}} - \sigma_{\text{tr}}, \mu_{\text{tr}} + \sigma_{\text{tr}}]$ as a confidence interval for the trace of the Hessian matrix.

The same procedure cannot be applied directly to propagate the uncertainty for the determinant of the Hessian matrix, $\det(H) = X_{xx} \cdot X_{yy} - X_{xy}^2$, which is a non-linear combination of random variables. Instead, we linearize the function $F(X_{xx}, X_{yy}, X_{xy}) = X_{xx} \cdot X_{yy} - X_{xy}^2$ by a first-order Taylor series approximation, $F \approx c + Js_3$[1]. Here, c is a constant that is disregarded in the propagation and J is the Jacobian matrix, containing the first-order partial derivatives of the function F, $J = [X_{yy}, X_{xx}, -2X_{xy}]$. The uncertainty can now be propagated as in the linear case, applying the Jacobian matrix to derive the standard deviation of the determinant

$$\sigma_{\text{det}}(X_{i,j}) = \sqrt{J\Sigma(s_3(X_{i,j}))J^{\text{T}}}, \tag{8}$$

associated with the mean $\mu_{\text{det}}(X_{i,j}) = F(\mu(s_3(X_{i,j})))$. The corresponding confidence interval for the determinant of the Hessian matrix is then $[\mu_{\text{det}} - \sigma_{\text{det}}, \mu_{\text{det}} + \sigma_{\text{det}}]$.

3.4. Indicator Functions

Notice that, as long as statistical parameters can be obtained for the multivariate random variable characterizing the data values at the grid points, uncertainty can be propagated to yield similar parameters for the gradient, and the trace and determinant of the Hessian matrix, irrespective of the probability distribution of the random variables.

We use the derived confidence region of the gradient at each grid vertex to indicate whether a critical point can occur around the respective grid location. For scalar data given at the vertices of a Cartesian grid, critical points can occur anywhere within a grid cell and are characterized by a zero gradient. We therefore derive positional indicators to relate the confidence region of the gradient to a zero magnitude. Then, as the Hessian matrix can be used to determine the type of a critical point, we use the confidence intervals of the trace and determinant of the Hessian to infer on the nature of the critical point at the given position.

Throughout the investigations, we use confidence intervals and avoid computing probabilities, because in this way we are independent of any probability distribution of the random variables. Furthermore, the applied procedures are deterministic and computationally inexpensive, needing neither the large computing times, nor the individually tailored number of trials to achieve a prescribed numerical tolerance that Monte Carlo integrations do.

3.4.1. Positional Indicator Functions

The mean and covariance matrix of the gradient vector at a grid vertex state, for the x and y gradient components, their means, dispersion around these means, and their coupling. The covariance matrix can define the shape of several confidence

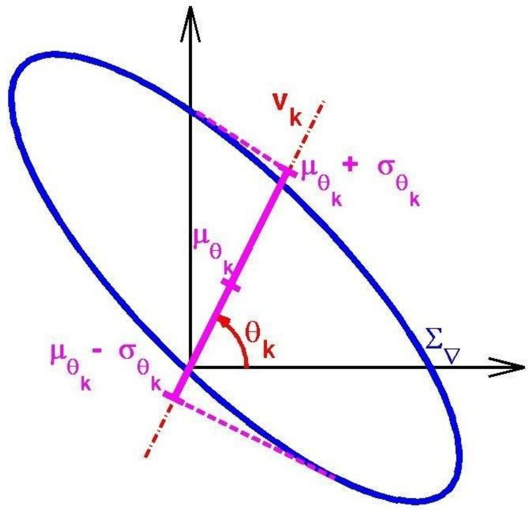

Figure 2: Projection of covariance matrix Σ_∇ on a direction v_k corresponding to angle θ_k, to yield a mean μ_{θ_k} and standard deviation σ_{θ_k}.

regions, which, depending on the desired confidence level, contain a certain percentage of the total probability distribution. A critical point can be considered to occur around a grid location if the origin falls within a prescribed confidence region. If no specific distribution is assumed, the confidence ellipse corresponding to the covariance matrix, $\mu_\nabla^{\text{T}} \Sigma_\nabla^{-1} \mu_\nabla \leq 1$, can be used to test whether the origin is a possible realization or not. In particular cases, such as the Gaussian distribution, confidence regions for arbitrary confidence levels can be considered, for instance, $\mu_\nabla^{\text{T}} \Sigma_\nabla^{-1} \mu_\nabla \leq 6.17$ for a 95.4% confidence level.

Based on the confidence region of the gradient at a grid vertex, but irrespective of the probability distribution that the gradient vector may follow, we have thus derived a binary indicator for the possibility of a critical point occurring at the grid vertex

$$\text{ind1}(x_{i,j}) = \begin{cases} 1 & \text{if } \mu_\nabla^{\text{T}} \Sigma_\nabla^{-1} \mu_\nabla \leq 1, \\ 0 & \text{otherwise.} \end{cases} \tag{9}$$

Because in Equation 9 we use the inverse of the covariance matrix, ill-conditioned matrices will cause spurious results. In such cases, instead of computing the Mahalanobis distance for the origin, we project the covariance matrix on every direction of a discretization of the unit circle $\theta_k \in [0, 2\pi]$ (cf. Figure 2). The projection yields a mean and a standard deviation

$$\mu_{\theta_k} = v_k^{\text{T}} \mu_\nabla, \tag{10}$$

$$\sigma_{\theta_k} = \sqrt{v_k^{\text{T}} \Sigma_\nabla v_k}, \tag{11}$$

which are then used to test whether every confidence interval contains the origin or not

$$\text{ind1}(x_{i,j}) = \begin{cases} 1 & \text{if } |\mu_{\theta_k}| \leq \sigma_{\theta_k}, \forall \theta_k \in [0, 2\pi], \\ 0 & \text{otherwise.} \end{cases} \tag{12}$$

Depending on the amount of information the user has on the data, the positional indicator can be refined, by considering the likelihood of the origin with respect to the covariance ellipse.

[1]For a highly non-linear function, other probabilistic approaches, such as a Monte Carlo simulation, would be preferred to a linearization of the function.

We illustrate this for the particular case of a Gaussian distribution, where the mean is the most likely value of the gradient. For the grid vertices where the origin falls inside the confidence ellipse, we compute the Mahalanobis distance to yield how far from the mean the origin lies in terms of the width of the ellipse in the direction of the origin. We then take its complement

$$\mathrm{ind1}(x_{i,j}) = \begin{cases} 1 - \sqrt{\mu_\nabla^\mathrm{T} \Sigma_\nabla^{-1} \mu_\nabla} & \text{if } \mu_\nabla^\mathrm{T} \Sigma_\nabla^{-1} \mu_\nabla < 1, \\ 0 & \text{otherwise.} \end{cases} \tag{13}$$

The values of the indicator can vary from one - the origin lies at the center of the confidence region, to zero - the origin lies on the boundary of the confidence region or outside of it.

The refined indicator assesses the likelihood of the origin, depending on its position with respect to the confidence ellipse. A zero mean indicates that the origin is the most probable realization of the gradient vector. Critical points are thus likely to occur around the given grid vertex throughout most of the ensemble members. The likelihood of the origin as a realization of the gradient decreases as the origin drifts from the center of the ellipse. Consequently, critical points occur less frequently around this location across the ensemble.

The indicator functions characterize the locations of the critical points and can be regarded as a measure of the positional stability of the critical points. Indicators have positive values in those regions where, according to the uncertainty analysis, critical points occur repeatedly throughout the ensemble. Nevertheless, a grid vertex where the positional indicator has a zero value does not mean that a critical point cannot appear around the grid vertex. While a critical point may still emerge, it is less likely to occur, e.g., it may be a transitory state or noise. Conversely, indicators may have positive values at grid points around which no critical point appears in any ensemble member. These reveal locations where critical points could have occurred in ensemble members that have not been realized. Furthermore, for specific distributions, the indicators may be refined to suggest, in addition to whether a critical point can occur around a vertex, the qualitative likelihood of an occurrence.

3.4.2. Type Indicator Functions

The previously derived indicators point out the possible locations where critical points occur frequently in the ensemble members. They do not, however, provide any information on whether a certain type of critical point could be expected around these positions. To obtain this kind of information, we need to go an order higher than the gradient, to the Hessian matrix and its associated eigenvalues: Only positive eigenvalues imply a local minimum, only negative eigenvalues a local maximum, whereas both positive and negative eigenvalues indicate a saddle. The nature of the critical points can be characterized statistically by summarizing either the eigenvalues of the Hessian matrix, or its trace and determinant. Because the function relating the second-order derivatives to the determinant is simpler than the function for the eigenvalues, we use the confidence intervals of the trace and determinant. From them, we derive type indicators showing the tendency of critical points appearing around a grid location to behave like a maximum, a minimum, or a saddle repeatedly throughout the ensemble.

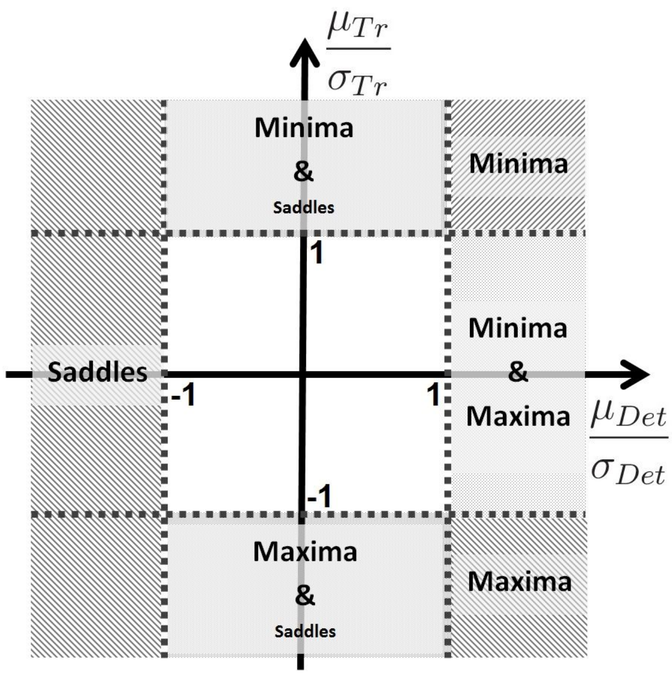

Figure 3: Classification of critical points showing stable behavior, depending on confidence intervals of trace and determinant.

Critical points can be classified according to the trace and determinant of the Hessian as follows: Depending on the sign of the determinant, we can distinguish between saddles, $\det(H) < 0$, and minima or maxima, $\det(H) > 0$. For the latter, the sign of the trace will further distinguish between minima, $\mathrm{tr}(H) > 0$, and maxima, $\mathrm{tr}(H) < 0$. According to this classification and the uncertainty analysis, critical points displaying a stable type of the behavior can occur around the grid vertices where the trace and the determinant of the Hessian can be considered as clearly positive or negative based on their confidence intervals (cf. Figure 3). We consider the trace (determinant) as *distinctly positive* if the lower endpoint of its confidence interval is greater than zero, $\mu - \sigma > 0$ (or $\mu/\sigma > 1$), and as *distinctly negative* if the upper endpoint is less than zero, $\mu + \sigma < 0$ (or $\mu/\sigma < -1$).

We begin with an analysis based on the trace of the Hessian matrix, for which the propagation of uncertainty necessitates no linearization and is unbiased. The trace of the Hessian matrix is simply the divergence of the gradient vector field; a clearly positive (negative) value of the divergence indicates that a critical point occurring around the given position tends to behave like a minimum (maximum) or, potentially, a saddle. More specifically, a divergence deemed as distinctly positive at a certain location indicates that, if a critical point appears at the location, it is unlikely that it is a maximum. A minimum has both eigenvalues positive and thus a positive divergence of the gradient, whereas a maximum has both eigenvalues negative and a negative divergence. Saddles, on the other hand, have both positive and negative eigenvalues, and the divergence can take both positive and negative values, depending on which eigenvalue is larger in absolute value. Because saddles may display negative or zero divergence, they are less likely to occur near locations with clearly positive divergence than minima are. Nevertheless, to be able to distinguish between minima and saddles, we need to take the sign of the determinant into account. Depending on whether the determinant can be regarded as clearly positive or negative, the critical point will most likely be a minimum or a saddle. Otherwise, a clear distinction is not possible, although minima are more likely. A similar analysis can be performed for a critical point around a position showing a clearly negative divergence: The critical point is expected to be a maximum, a saddle, or both, depending on the determinant of the Hessian.

An analysis based solely on the trace of the Hessian indicates locations where predominantly minima (maxima) and possibly saddles emerge. Taking the determinant into account can further differentiate between minima (maxima) and saddles. Vice-versa, an analysis based only on the determinant of the Hessian points out locations with either saddle or minimum/maximum behavior. The trace of the Hessian is in this case used to potentially distinguish between stable minima and maxima.

The type indicators can also be refined for particular probability distributions. In the case of a Gaussian distribution, we can identify locations with an almost zero divergence, where only saddle points should be expected. A grid point is considered to have a very small divergence if zero is less than a certain threshold τ away from μ_{Tr} in terms of σ_{Tr}, i.e., $|\mu_{\mathrm{Tr}}|/\sigma_{\mathrm{Tr}} < \tau$.

If the positional indicators suggest the spatial positions where critical points appear in the ensemble, the type indicators point out whether a stable behavior can be expected at any of these locations. At grid points where a stable sign can be assumed for both the trace and the determinant of the Hessian, critical points of the same type are likely to occur. The user can expect a specific type of critical point and of surface behavior around the grid points throughout the ensemble. If just one of the quantities shows a stable sign, certain variations in type can be expected. While minima (maxima) are still more likely than saddles for a stable sign of the trace, no distinction between maxima and minima can be made for a stable sign of the determinant. If no exact statement can be made on the sign of any of the two quantities, according to the uncertainty analysis, any type of critical point may appear around the location. This indicates a highly unstable surface behavior at the given spatial location in the ensemble.

It is worth mentioning that, even though the proposed methods are presented for the 2D case, the extension to 3D is straightforward. Due to space considerations, however, we do not give the mathematical derivations for 3D, but only briefly illustrate possible 3D visualizations in Section 4.

4. Visualization

In the following, we present techniques to illustrate the introduced indicators together with the scalar fields of the ensemble. We occasionally display the critical points, even though they are not relevant to computing the indicator functions, in order to contribute to the validation of the proposed techniques. Furthermore, the concurrent visualization allows us to place the indicators and the critical points in space, and observe the possible occurrences of critical points and their type stability together with various related surface components.

Visual outputs have the scalar fields in the background, either as contour plots or texture maps on a zero-elevation surface, the used colormap consisting of shades of blue (for low values) and green (for high values). We use a rather low number of shades, in order to avoid smooth transitions between colors and thus convey to a certain extent different surface components when using texture maps. Depending on the interests of the user, the visualization techniques can be extended to integrate further surface components, but, since these are specific to the user's needs, we do not do so here. Critical points, if shown, are drawn as circles, colored either in black, when the type information is not relevant, or depending on the type of the critical points: Saddles maintain their black color, maxima are colored in orange, and minima in pink.

4.1. Visualization of Positional Indicators

Positional-related indicators are encoded via gray-colored circular glyphs, centered at every vertex of a Cartesian grid. To avoid clutter, the circular glyphs have radii equal to half of the length of a grid cell's side. We prefer a glyph-based to a point-based representation, because it reflects better the fact that critical points occur around and not exactly at the grid vertices. The visualization is more dense and thus more likely to cover the actual positions of the critical points. It also serves to emphasize the locations where critical points occur. In the following, we denote the connected areas where the indicators take positive values as emphasized or marked regions.

For the refined positional indicators, we encode the complement of the Mahalanobis distance in the opacity of the glyph: The more opaque the glyph, the more likely it is that critical points occur repeatedly around the grid vertex throughout the ensemble. Both types of positional indicators are illustrated in Figures 4(a) and (b), showing the mean field of a temperature ensemble, simulated by the European Center for Medium-Range Weather Forecast (ECMWF) for a forecast period of nine days above Europe. The general indicators are displayed in Figure 4(c), along with every critical point of the ensemble. It can be observed that the locations where critical points actually occur in the ensemble agree with those marked by the indicators.

Representing the possible locations of critical points via the positional indicators has several benefits over simply displaying the critical points of the ensemble. Firstly, deriving and displaying the indicators is a computationally inexpensive technique to highlight the regions where critical points tend to occur predominantly in the ensemble and requires no tailoring compared to various clustering algorithms. It also needs little to no effort on the user's side. Furthermore, the indicators reflect the variability induced by uncertainty on the positions of critical points, marking locations around which critical points are expected to appear consistently in the ensemble. Thus, regions that are emphasized, but contain no critical points, indicate locations where critical points could have occurred in further ensemble members that have not been realized. Conversely, regions that have not been marked and still contain critical points, suggest that

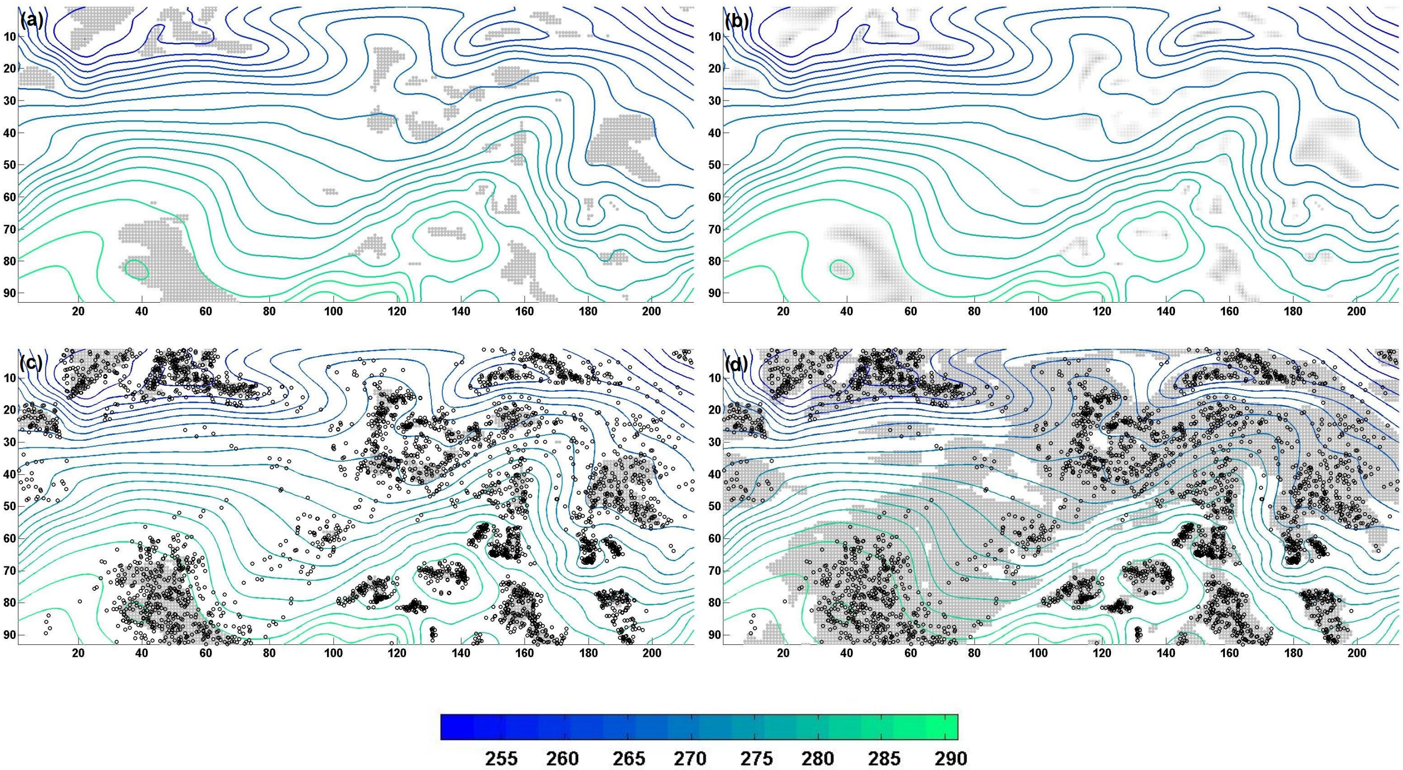

Figure 4: Iso-contours of mean scalar field with positional indicator functions: (a) General and (b) refined indicators for confidence ellipse given by covariance matrix. (c) General indicators with all critical points. (d) General indicators for confidence level of 95.4% with all critical points.

such unstable critical points are less likely to occur. Moreover, in particular cases, e.g., a Gaussian distribution, we can further improve the stability assessment and distinguish between the most stable regions - where critical points are likely to occur in most ensemble members, and the least stable regions - where critical points occur only occasionally.

Finding the regions holding the most stable critical points is useful when the occurrence of certain events or features is strictly related to the existence of critical points. It is also relevant as a first step to rapidly identify the locations and isovalues that deserve further investigation.

Assuming a Gaussian distribution for the current example, emphasized regions may occupy larger areas when confidence regions with higher confidence levels are considered. Figure 4(d) shows the positional indicators for a confidence level of 95.4%. Just a few critical points are outside of the covered regions or, vice-versa, critical points are not expected to occur in unmarked areas. Moreover, critical points that appear in regions marked in (d), but not in (c), are less likely to emerge consistently than those in regions marked in both figures.

Figures 4(a)-(d) have the mean scalar field as a background. We could have nonetheless used any other ensemble member instead, since the mean scalar field is only relevant to illustrate the ensemble behavior for particular distributions of the random variables, such as the Gaussian distribution. In fact, displaying the circular glyphs representing the indicators over the individual ensemble members and their critical points classifies critical points as stable or unstable. Moreover, in the Gaussian case, the user can interactively classify the critical points from most to least stable by means of a slider functionality: As α varies in the right hand side of $\mu_\nabla(x_{i,j})^{\mathrm{T}}\Sigma_\nabla(x_{i,j})^{-1}\mu_\nabla(x_{i,j}) \leq \alpha$ from 0 to 9.21 (corresponding to a confidence level of 99%), more and more circular glyphs cover the critical points of the ensemble member; the lower the value of α that first results in a critical point being covered, the more stable the critical point. Critical points left uncovered for $\alpha \geq 9.21$ are classified as unstable according to the uncertainty analysis.

Illustrating the possible locations of the critical points via the indicators is more revealing than simply displaying critical points of individual ensemble members or of their mean scalar field. While in particular cases the mean field is illustrative of the ensemble behavior, its critical points do not provide the same insight as that offered by the indicators. First of all, the critical points of the mean data set do not necessarily occur in every region emphasized by the indicators (cf. Figure 5). Secondly, while these critical points reveal locations around which critical points may be expected, they indicate neither the shape, nor the extent of the regions where critical points may occur.

Similar techniques can be applied to visualize the potential locations of critical points in 3D. We illustrate this in Figure 6 for the 3D temperature ensemble for which the aforementioned 2D data set is the slice at the highest pressure level. Spherical glyphs, the direct extension of the circular glyphs in 2D, are shown immersed in the partly transparent volume data in Figure 6(a). Then, from a volume data containing at each grid vertex the Mahalanobis distance $\mu_\nabla^{\mathrm{T}}\Sigma_\nabla^{-1}\mu_\nabla$ of the origin from the gradient mean, we extract in Figure 6(b) the iso-surface of iso-value 1, which we color depending on the values of the scalar field at

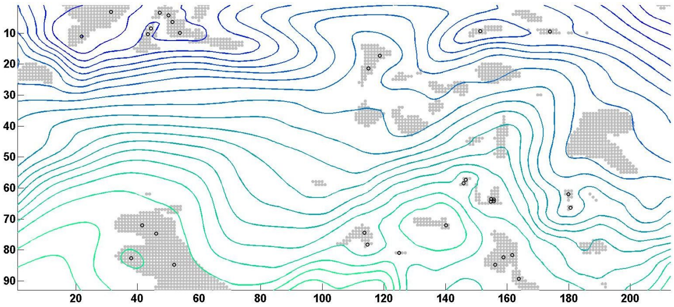

Figure 5: Critical points of the mean scalar field with positional indicators for confidence ellipse given by covariance matrix.

the vertices of the iso-surface. The most representative critical points of the ensemble are shown as red spheres.

4.2. *Visualization of Type Indicators*

The type indicators are encoded via colored circular glyphs: Glyphs for grid points where only the determinant of the Hessian matrix fulfills the specified criteria for a certain type are colored in purple, while those where only the trace of the Hessian fulfills the criteria are colored in brown, unless the determinant suggests saddle behavior when the trace indicates maximum (minimum) behavior. Such grid points are colored in gray. Finally, the glyphs where the criteria hold for both the determinant and the Hessian matrix, i.e., where critical points with the most stable behavior emerge, are colored in red.

All critical points of the ensemble are shown in Figure 7(a), colored according to their type. Figure 7(b) emphasizes regions where critical points tend to behave like maxima. Notice that regions with stable behavior are indicated mostly in the areas where critical points of the same type cluster together, as opposed to those comprising a mixture of critical points of different types. The type indicators offer nevertheless additional insight compared to the naive display of critical points colored according to their nature. For instance, both regions numbered 1 and 2 in Figure 7(b) appear to consist of three clusters of maxima and saddle points, for which a visual inspection would indicate stable maximum behavior in the middle of the first region, and the left and right thirds of the second region. According to the uncertainty analysis, however, only the second region shows both positive determinant and negative trace values, and thus a more likely maximum behavior. Nonetheless, both regions show clearly negative trace values, pointing out that minima are unlikely to occur, whereas maxima and potentially saddle points can be expected around the indicated regions.

Compared to regions 1 and 2, a clear separation between critical points of different types is more difficult to do visually in region 3. The type indicators suggest that maxima and, possibly, saddles are likely to appear in the upper half of the region, while maxima and minima can be expected in the lower half. Critical points occurring around three grid vertices display stable maximum behavior.

Spatial positions suggesting critical points with predominantly saddle behavior are displayed in Figure 7(c). Although critical points of different types occur in both regions numbered 1 and 2, the type indicators reveal locations around which saddle points can be expected to occur frequently. Figure 7(d) shows grid vertices around which primarily minima are expected to emerge. Notice that, even though grid points in regions numbered 1 and 2 have distinctively positive trace values, their clearly negative determinant values suggest saddle points instead of minima as more likely to occur there. Figure 7(a) indicates that saddle points indeed prevail in the two areas.

5. Validation

In the previous sections we introduced and visualized two types of functions to indicate, at each grid vertex, whether critical points can be assumed to emerge nearby and display a stable behavior. Depending on the indicators, critical points have been classified as more or less stable in location and type.

According to this classification, critical points occurring near grid vertices where positional indicators have positive values are stable, i.e., they are more likely to appear frequently around the same position in the ensemble members. The so-called unstable points are less likely to occur, i.e., they may be numerical noise or a transitory configuration. Furthermore, positive indicator values for those grid vertices around which no critical points appear suggest locations where critical points may appear in further realizations of the ensemble.

To validate our techniques, we want to relate the number of occurrences of a critical point around a certain position with its classification as stable or unstable. This is nonetheless difficult, since critical points do not generally occur at the same spatial location. Even assigning critical points to grid points does not typically result in a significant increase in the number of ensemble members where a grid vertex gets assigned at least one critical point, because critical points may be assigned to different neighboring grid points. We alleviate this problem by assigning a critical point to all the vertices at the corners of the grid cell where the critical point resides. Then, we build a 2D histogram that counts, for each grid vertex, the number of ensemble members where at least one critical point was assigned to the vertex. Starting with the peak of the histogram in descending order, we check, for all the grid points having the given histogram value, the percentage of points that do not have positive indicator values, i.e., the grid points to which critical points have been assigned, but have not been marked by the indicators as well. This yields, for each histogram value, the percentage of false negatives. We can perform a similar analysis for false positives, computing the percentage of points that have positive values of the indicators, but zero histogram values, i.e., the grid points that have been marked by the indicators, but to which no critical points have been assigned. Note that the grid points considered in the false negative and false positive analysis do not sum up to the total number of grid points.

The false negative error rates for the previous 2D example are shown in Table 1. Figure 8 shows the mean scalar field with the positional indicators and the six grid points that have the five highest histogram values, numbered from 1 to 5 in decreasing order. The grid point numbered 1, at the peak of the histogram, is marked in 56% of the ensemble members and has a positive

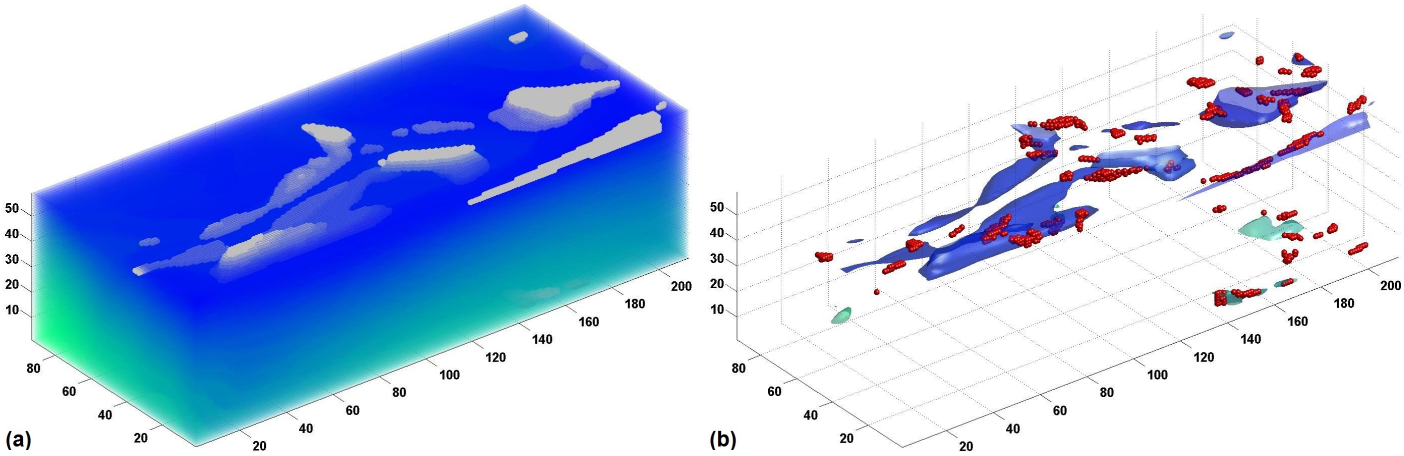

Figure 6: 3D temperature ensemble showing positional indicators via (a) gray-colored spherical glyphs and (b) iso-surface of iso-value 1, along with critical points shown as red spheres in the latter figure.

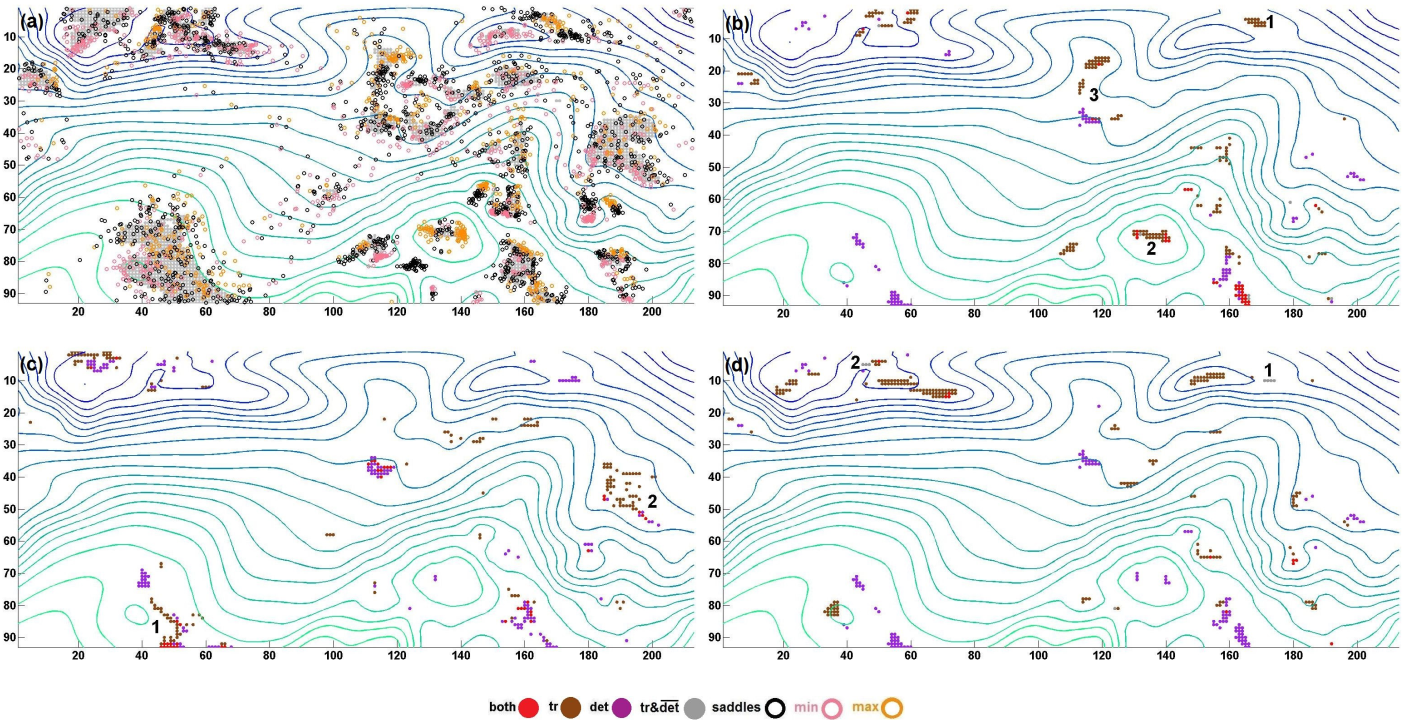

Figure 7: Iso-contours of mean scalar field of temperature ensemble with type indicator functions and critical points. (a) Critical points of the ensemble. Indicators only for (b) maxima, (c) saddle points, and (d) minima.

indicator value. Notice that three other of its neighboring vertices also have high histogram values, although only grid points numbered 4 and 5 have positive indicator values. Critical points in the grid cell given by the four vertices can be assumed stable, i.e., they occur frequently in the cell within the ensemble members, but the frequency can be expected to decrease in the lower right direction. Comparable observations can be made for the two grid points numbered 3: Both vertices are marked in 46% of the ensemble members, but only the lower grid point (black-colored in Figure 8) shows a positive indicator value. Critical points are thus less likely to emerge in the upper direction. Such grid points, with zero indicator values, but neighboring vertices with positive indicator values, cause the positive false negative error rates at the beginning of the table. False negative error rates increase towards the end of the table, revealing the grid points around which critical points appear less frequently. The shown error rates are in fact upper bounds of the actual values, because critical points are assigned to all their neighboring grid points, but not every grid point is marked by the indicators.

The results show that grid vertices around which critical points occur most often are also marked by the indicators. Regarding the false positives, 12% of the 2019 vertices with positive indicator values did not get any critical points assigned. For specific distributions, increasing the confidence level would result in a larger coverage of the indicators, i.e., lower false negative rates, but higher false positive rates.

H	n	r	H	n	r
0.56	1	0	0.22	15	0.33
0.5	1	1	0.2	19	0.58
0.46	2	0.5	0.18	27	0.52
0.4	1	0	0.16	33	0.3
0.38	1	0	0.14	62	0.21
0.34	2	0	0.12	105	0.29
0.32	3	0	0.1	183	0.36
0.3	2	0.5	0.08	352	0.41
0.28	3	0.67	0.06	676	0.54
0.26	5	0.4	0.04	1344	0.66
0.24	12	0.17	0.02	2868	0.84

Table 1: False negative analysis for temperature ensemble. H - histogram value, normalized by number of ensemble members; n - number of grid points holding histogram value; r - error rate.

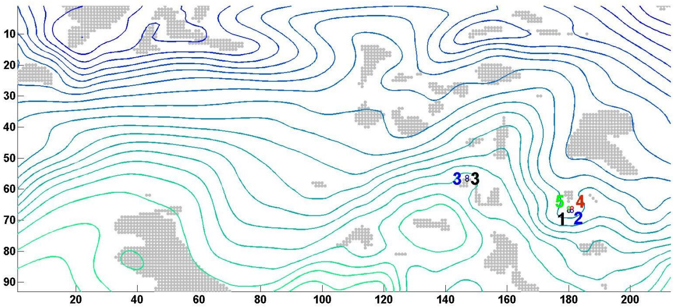

Figure 8: Mean scalar field with positional indicators and the grid points holding the five highest histogram values, numbered from 1 to 5.

6. Further Results

We apply the introduced techniques for analysis, visualization, and validation to three other data sets, two synthetic ensembles and another ECMWF ensemble.

The first synthetic data set, of dimensions 100 x 100, was generated by assigning the three parameters a, b, and c in $-x^4/4-y^4/4-x^2y^2/2+ax^2/2+bxy+cy^2/2, (x,y) \in [-2,2]X[-2,2]$, random numbers generated from a multivariate normal distribution with the following mean and covariance matrix

$$\mu = \begin{bmatrix} 0.5 \\ 1 \\ 0.5 \end{bmatrix}, \; \Sigma = \begin{bmatrix} 1 & -0.5 & 0.5 \\ -0.5 & 1 & -0.5 \\ 0.5 & -0.5 & 1 \end{bmatrix}.$$

When the parameters take on the values in the mean vector, there are three critical points, a saddle at $(0,0)$ and two maxima at $(\sqrt{0.75}, \sqrt{0.75})$ and $(-\sqrt{0.75}, -\sqrt{0.75})$. Figure 9 illustrates the results for the first 50 members of an ensemble comprising 5000 members, where the considered confidence ellipse was that corresponding to the covariance matrix. The refined positional indicators, shown in Figure 9(a) (assuming a Gaussian distribution fits the data), cover many of the critical points, especially around the critical points of the mean. In Figure 9(b), several grid points situated around the maxima of the mean show clearly positive determinant and negative trace values, i.e., stable maximum behavior. The rest of the grid points display only definitely negative trace values, which means that saddles should not be excluded around these locations, although maxima are more likely. No vertex with a dominant minimum behavior is found, since the clearly positive determinant values shown in Figure 9(c) only exclude saddles and, according to Figure 9(b), indicate maximum behavior. Minima appear occasionally only around the origin. Even though critical points are present around the origin in every ensemble member and the positional indicators show positive values there, no stable type behavior can be identified in the region. This happens because saddle points also occur around the origin, although neither frequently enough to cause distinctly negative determinant values, nor with predominantly positive trace values. Grid points with small trace values ($\tau = 0.1$), around which saddle points are expected to occur, are shown in Figure 9(d).

H	1	0.04	0.02
n	4	50	476
r	0.5	0.48	0.40

Table 2: False negatives for first synthetic data set (50 ensemble members).

N	50	100	500	1000	2500	5000
R	0.84	0.71	0.33	0.15	0.02	0.001

Table 3: False positives for first synthetic data set. N - number of ensemble members; R - false positive error rate.

Table 2 shows the results of the false negative analysis. The four grid points that make the peak of the histogram, two of which have positive indicator values, are located around the origin. Notice that critical points are identified around the origin in all ensemble members. Furthermore, these critical points appear mostly on the secondary diagonal of the square, near the two grid points with positive indicator values. The other two grid points with maximum histogram values have non-positive indicator values, since critical points do not occur around them. Their high histogram value is due to the critical points having been assigned to all neighbors. Except for these critical points, however, all other critical points are rather scattered, reason for which no other grid point is marked in more than two ensemble members. According to the false negative error rate, nonetheless, the grid points near which more critical points appear have positive indicator values.

Due to the low number of critical points and their scattering, the false positive error rate is very high (84%). Nevertheless, the grid points around which no critical points occur, but which display positive indicator values, suggest locations where critical points may appear in further realizations of the ensemble. To illustrate this, we consider all the 5000 ensemble members. At the peak of the histogram the situation is unchanged, showing that the tendency of critical points to occur on the secondary rather than main diagonal of the square had been captured well previously. While critical points are still scattered (except for the grid points in the vicinity the origin, no other vertex is marked in more than 64 ensemble members), they cover more densely the regions emphasized by the indi-

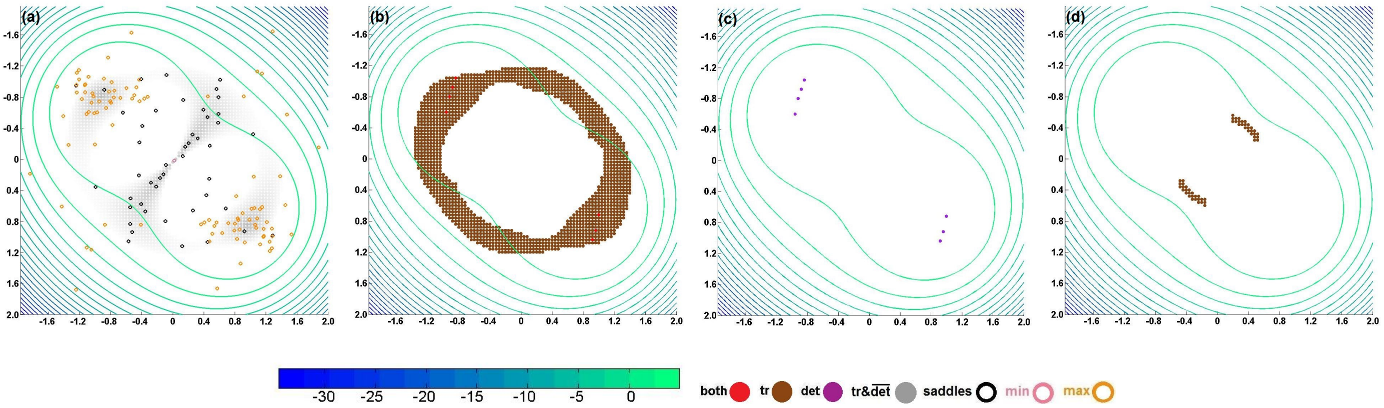

Figure 9: Iso-contours of mean scalar field of first synthetic data set with indicators. (a) Refined positional indicators with all critical points. (b) Type indicators for maxima. (c) Type indicators for minima. (d) Type indicators for saddle points.

H	n	r	H	n	r
0.24	1	0	0.12	9	0.44
0.22	1	0	0.1	15	0.87
0.2	3	0.67	0.08	38	0.76
0.18	1	0	0.06	47	0.81
0.16	3	0	0.04	46	0.89
0.14	1	0	0.02	97	0.99

Table 4: False negative analysis for second synthetic data set.

cators. Consequently, the false positive rate decreases dramatically to 0.1%. The decreasing trend of the error rate for increasing numbers of ensemble members is shown in Table 3.

A second synthetic data set, also of dimensions 100 x 100, was generated by assigning the parameter ω in $x^3+y^3-\omega xy-x-y=0, (x,y)\in[-2,2]X[-2,2]$, random numbers generated from a normal distribution with a zero mean and standard deviation of 2. Depending on the value of ω, there should be either four (two nodes and two saddles for $-2<\omega<2$), three (two nodes and a saddle for $\omega=\pm 2$), or two critical points (a node and a saddle for $\omega<-2$ or $2<\omega$).

The mean scalar field, together with the positional and type indicators, and all critical points, is shown in Figures 10(a)-(c). The badly-scaled covariance matrices of the gradients cause spurious results for the positional indicators (cf. Figure 10 (a)), which now cover the whole domain with no distinct pattern, even though critical points occur mostly on the main diagonal. Nonetheless, it does not affect the type indicators (cf. Figures 10 (b) and (c)), which still identify the maximum behavior in the upper triangular part and the minimum behavior in the lower triangular part. Projecting the covariance matrix (cf. Figures 10(d)-(f)) results in positional indicators that cover mostly areas where critical points are identified. Both false positive (13% for 45 marked grid points) and negative error rates (cf. Table 4) are correspondingly low.

For our last example we use data from the ECMWF Ensemble Prediction System (EPS), ECMWF's operational ensemble weather forecast system. The EPS produces forecasts twice daily and includes 50 members and a control run. For more details on the system, we refer the reader to, for instance, [37]. Here we use the forecast initialized on October 17, 2012. The data has been interpolated horizontally from the model grid to a regular latitude/longitude grid with a grid spacing of 0.3 degrees in both dimensions, and vertically to levels of constant pressure. The selected scalar field is the 60 hour forecast of the geopotential height field at a pressure level of 1000 hPa, valid on October 19, 2012.

Figure 11 shows the geolocated mean scalar field, where low altitudes of the pressure surface are colored in shades of blue and high altitudes in shades of green. A distinct low pressure system is visible south of Greenland, several critical points appearing there. Critical points are useful in this context to help identify features related to adverse weather conditions, such as cyclonic centers. Cyclonic features can be located by using a mixture of techniques, among which the detection of well-defined geopotential minima. Since data is inherently affected by uncertainty, it is relevant to point out the spatial locations around which pressure minima are to be expected and which should be further investigated.

Positional indicators are shown in Figure 11(a) for a confidence ellipse corresponding to a 95.4% confidence level. The indicators cover the majority of areas where critical points occur, including the region displaying the low pressure. False negative error rates are therefore low, many of them under 20%, while the false positive rate is 37%. Type indicators showing stable minimum behavior are shown in Figure 11(b). The upper left corner of the region has several grid points with clearly positive trace values, but no definitely positive determinant values and even five grid points with clearly negative determinant values, i.e., while minima are the most likely type of critical points to appear in the region, saddle points should not be excluded, especially around the five grid points.

7. Conclusion

Prominent features display variations across ensembles, potentially changing their location and shape. In this paper, we developed several indicator functions to give insight into the

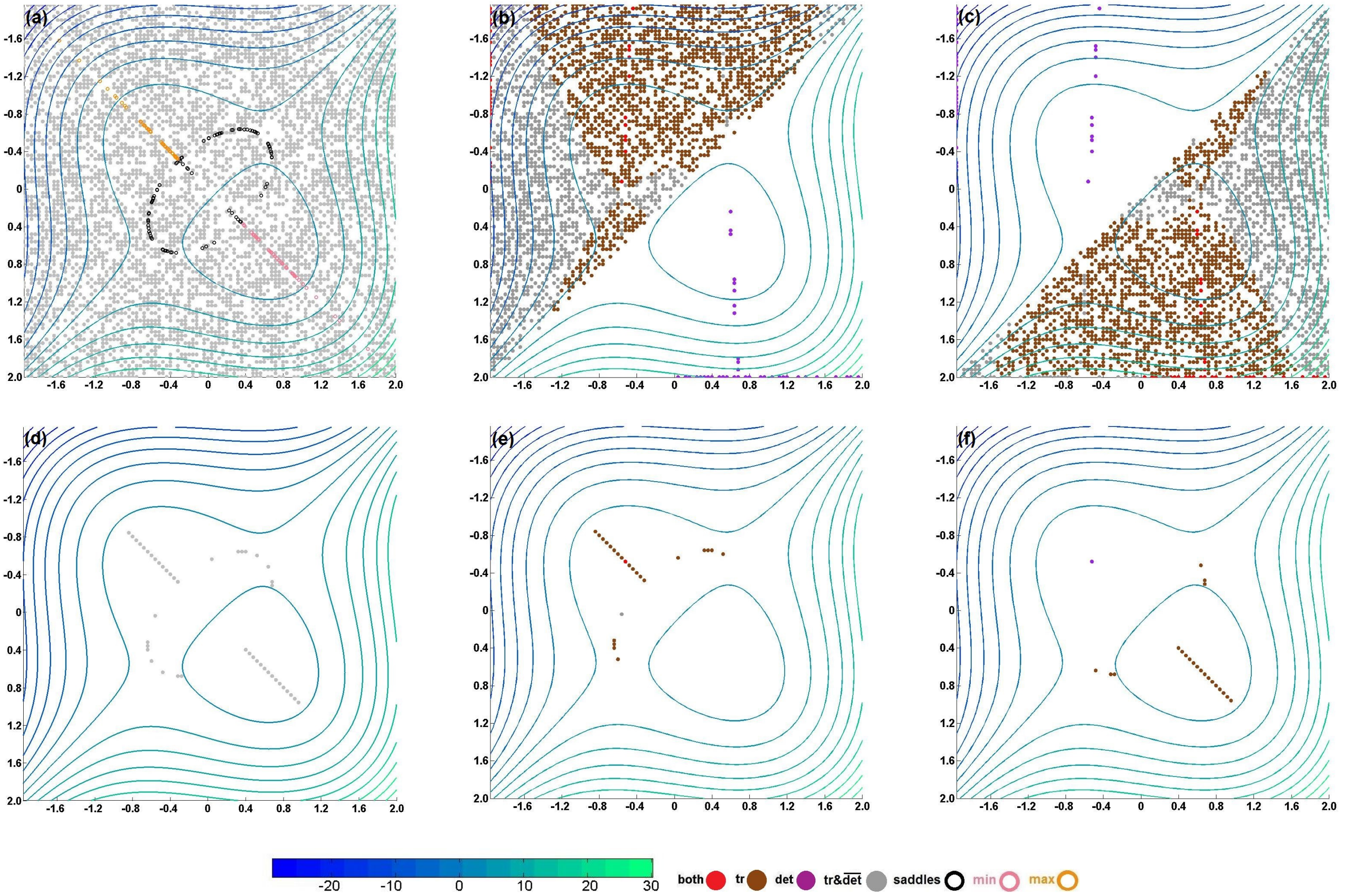

Figure 10: Iso-contours of mean scalar field of second synthetic data set with indicators. (a) Positional indicators and all critical points. (b) Type indicators for maxima. (c) Type indicators for minima. (d) Modified positional indicators. (e) Type indicators for maxima after modification. (f) Type indicators for minima after modification.

salient features of scalar fields and their stability, by investigating their associated critical points. We summarized ensembles statistically and computed corresponding moments for the associated gradient fields and the determinant and trace of the Hessian matrices. The first were used to derive quantities indicating the likelihood of existence of a critical point at a given location, whereas the latter reveal whether the critical point tends to behave consistently like a minimum, a maximum, or a saddle. We then presented techniques to visualize the proposed indicators simultaneously with the scalar fields and several of their surface components. Finally, we applied the methods on two synthetic and two real world data sets, to illustrate how the proposed methods emphasize the possible critical points and their stability in behavior in ensembles of uncertain scalar fields.

Positional indicators based on confidence intervals of gradients show the locations where critical points tend to occur repeatedly within ensemble members. Critical points already indicate within one ensemble member the relevant iso-values where topological changes of the iso-contours occur: Contour components emerge at minima, disappear at maxima, split or merge at saddles. The positional indicators can be regarded as a fast and computationally inexpensive method to point out the locations and iso-values that are significant for the ensemble according to the uncertainty analysis. Depending on the size of the ensemble, some of the indicated positions are not related to the available ensemble members, as the indicators may mark grid points with no critical points occurring in the immediate vicinity. However, such locations were shown to be suggestive for ensemble members that have not been realized.

The type indicators characterize the behavior of critical points and suggest the manner in which interesting associated surface components (iso-contours and various regions grown around critical points) develop. For instance, a location indicating a critical point that tends to behave like a minimum shows a stable structure, in the sense that the critical point, the region grown around it, and the topological event of a surface component emerging persist throughout the ensemble members. On the other hand, a spatial position with no specific type behavior indicates a potentially unstable structure, whose shape inverts across the ensemble, even though the structure may be present in most ensemble members. Conclusions on the stability of the associated features are harder to draw when the uncertainty analysis allows the clear exclusion of only one type of critical point behavior. The type indicators are also useful in appli-

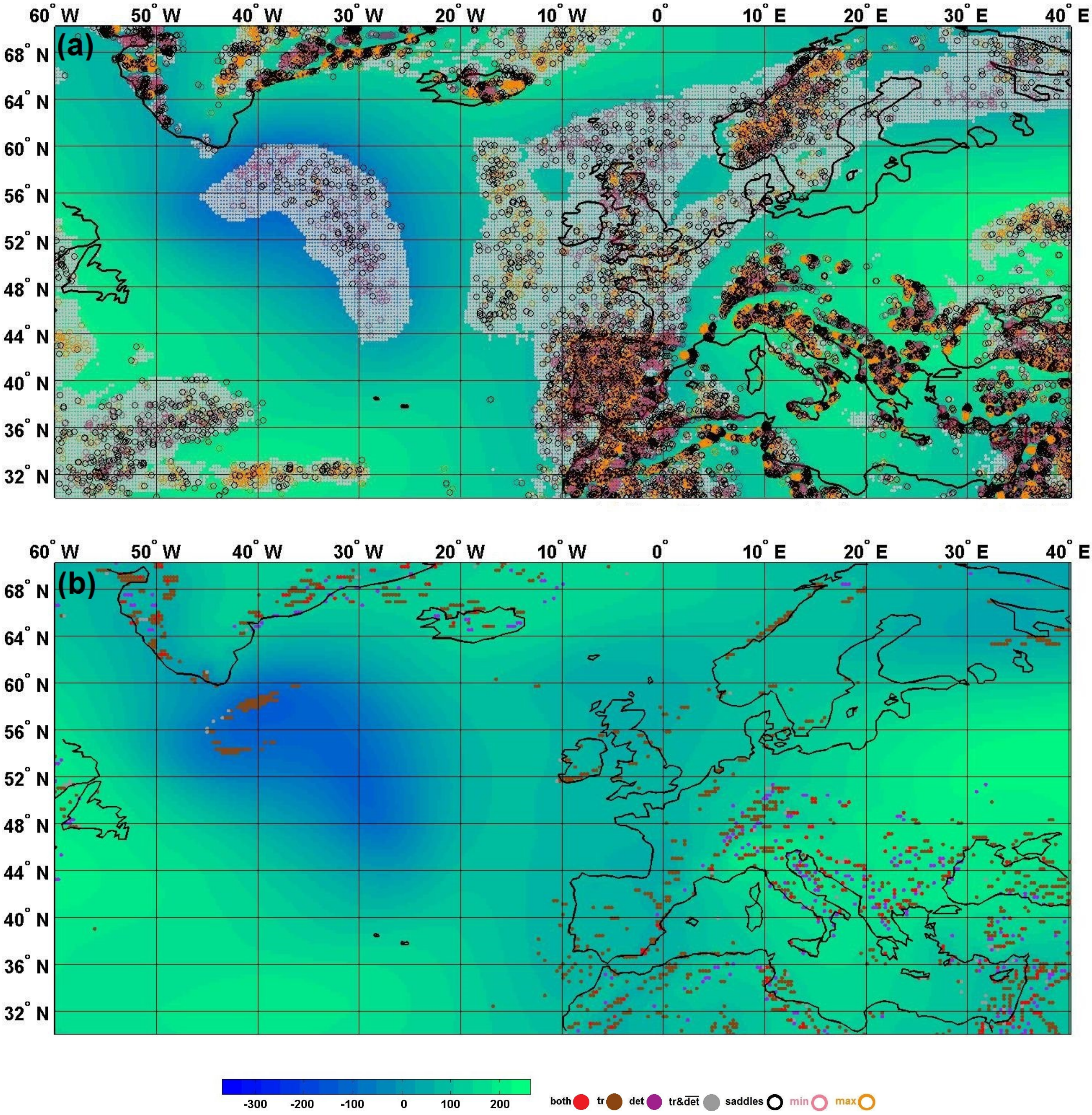

Figure 11: Mean scalar field of temperature ensemble with indicator functions. (a) Positional indicators with all critical points. (b) Type indicators for minima.

cations where locating stable critical points of a certain type is relevant to the detection and tracking of various features, e.g., pressure minima are used in meteorological applications to identify cyclonic features.

There are several possible directions for future work: Firstly, the notion of stability of critical points could be extended, to allow tracking critical points (and associated features) from one ensemble member to another. Furthermore, similar investigations could be performed for uncertain vector fields. It would be interesting to develop the analysis to assess the stability of the entire topology of the vector fields, in addition to the critical points.

Acknowledgments

The work was partly funded by the European Union under the ERC Advanced Grant 291372: Safer-Vis - Uncertainty Visualization for Reliable Data Discovery. We thank Tobias Pfaffelmoser for valuable discussions during the development of the work described here. Access to ECMWF prediction data has been kindly provided in the context of the ECMWF special project "Support Tool for HALO Missions". We are grateful to the special project members Marc Rautenhaus and Andreas Dörnbrack for providing the ECMWF EPS dataset of October 17, 2012.

References

[1] Pfaffelmoser T, Reitinger M, Westermann R. Visualizing the positional and geometrical variability of isosurfaces in uncertain scalar fields. In: Computer Graphics Forum; vol. 30. Wiley Online Library; 2011, p. 951–60.
[2] Pothkow K, Hege HC. Positional uncertainty of isocontours: Condition analysis and probabilistic measures. Visualization and Computer Graphics, IEEE Transactions on 2011;17(10):1393–406.
[3] Wu K, Zhang S. A contour tree based visualization for exploring data with uncertainty. International Journal for Uncertainty Quantification 2013;3(3).
[4] Pfaffelmoser T, Mihai M, Westermann R. Visualizing the variability of gradients in uncertain 2d scalar fields. IEEE transactions on visualization and computer graphics 2013;.
[5] Griethe H, Schumann H. The visualization of uncertain data: Methods and problems. In: SimVis. 2006, p. 143–56.
[6] Thomson J, Hetzler E, MacEachren A, Gahegan M, Pavel M. A typology for visualizing uncertainty. In: Proc. SPIE; vol. 5669. 2005, p. 146–57.
[7] Potter K, Rosen P, Johnson CR. From quantification to visualization: A taxonomy of uncertainty visualization approaches. In: Uncertainty Quantification in Scientific Computing. Springer; 2012, p. 226–49.
[8] Wittenbrink C, Pang A, Lodha S. Glyphs for visualizing uncertainty in vector fields. Visualization and Computer Graphics, IEEE Transactions on 2002;2(3):266–79.
[9] Djurcilov S, Kim K, Lermusiaux P, Pang A. Visualizing scalar volumetric data with uncertainty. Computers & Graphics 2002;26(2):239–48.
[10] Rhodes P, Laramee R, Bergeron R, Sparr T. Uncertainty visualization methods in isosurface rendering. In: Eurographics. Citeseer; 2003, p. 83–8.
[11] Lundstrom C, Ljung P, Persson A, Ynnerman A. Uncertainty visualization in medical volume rendering using probabilistic animation. Visualization and Computer Graphics, IEEE Transactions on 2007;13(6):1648–55.
[12] Sanyal J, Zhang S, Dyer J, Mercer A, Amburn P, Moorhead R. Noodles: A Tool for Visualization of Numerical Weather Model Ensemble Uncertainty. IEEE Transactions on Visualization and Computer Graphics 2010;.
[13] Pang AT, Wittenbrink CM, Lodha SK. Approaches to uncertainty visualization. The Visual Computer 1997;13:370–90.
[14] Zehner B, Watanabe N, Kolditz O. Visualization of gridded scalar data with uncertainty in geosciences. Computers & Geosciences 2010;.
[15] Grigoryan G, Rheingans P. Point-based probabilistic surfaces to show surface uncertainty. Visualization and Computer Graphics, IEEE Transactions on 2004;10(5):564–73.
[16] Brown R. Animated visual vibrations as an uncertainty visualisation technique. In: GRAPHITE. ACM. ISBN 1581138830; 2004, p. 84–9.
[17] Pfaffelmoser T, Westermann R. Visualization of global correlation structures in uncertain 2d scalar fields. In: Computer Graphics Forum; vol. 31. Wiley Online Library; 2012, p. 1025–34.
[18] Pfaffelmoser T, Westermann R. Correlation visualization for structural uncertainty analysis. International Journal for Uncertainty Quantification 2013;3(2).
[19] Pöthkow K, Weber B, Hege HC. Probabilistic marching cubes. In: Computer Graphics Forum; vol. 30. Wiley Online Library; 2011, p. 931–40.
[20] Theisel H, Rössl C, Weinkauf T. Topological representations of vector fields. In: Shape Analysis and Structuring. Springer; 2008, p. 215–40.
[21] Laramee RS, Hauser H, Zhao L, Post FH. Topology-based flow visualization, the state of the art. In: Topology-based methods in visualization. Springer; 2007, p. 1–19.
[22] Scheuermann G, Tricoche X. Topological methods for flow. The Visualization Handbook 2005;:341.
[23] Thompson D, Levine J, Bennett J, Bremer PT, Gyulassy A, Pascucci V, et al. Analysis of large-scale scalar data using hixels. In: Large Data Analysis and Visualization (LDAV), 2011 IEEE Symposium on. 2011, p. 23–30. doi:10.1109/LDAV.2011.6092313.
[24] Otto M, Germer T, Hege HC, Theisel H. Uncertain 2d vector field topology. In: Computer Graphics Forum; vol. 29. Wiley Online Library; 2010, p. 347–56.
[25] Petz C, Pöthkow K, Hege HC. Probabilistic local features in uncertain vector fields with spatial correlation. In: Computer Graphics Forum; vol. 31. Wiley Online Library; 2012, p. 1045–54.
[26] Pöthkow K, Hege HC. Nonparametric models for uncertainty visualization. Computer Graphics Forum 2013;32(3pt2):131–40. URL: http://dx.doi.org/10.1111/cgf.12100. doi:10.1111/cgf.12100.
[27] Bhatia H, Jadhav S, Bremer PT, Chen G, Levine JA, Nonato LG, et al. Edge maps: Representing flow with bounded error. In: Pacific Visualization Symposium (PacificVis), 2011 IEEE. IEEE; 2011, p. 75–82.
[28] Schultz T, Theisel H, Seidel HP. Topological visualization of brain diffusion mri data. Visualization and Computer Graphics, IEEE Transactions on 2007;13(6):1496–503.
[29] Edelsbrunner H, Letscher D, Zomorodian A. Topological persistence and simplification. In: Foundations of Computer Science, 2000. Proceedings. 41st Annual Symposium on. IEEE; 2000, p. 454–63.
[30] Dey TK, Wenger R. Stability of critical points with interval persistence. Discrete & Computational Geometry 2007;38(3):479–512.
[31] Reininghaus J, Kotava N, Gunther D, Kasten J, Hagen H, Hotz I. A scale space based persistence measure for critical points in 2d scalar fields. Visualization and Computer Graphics, IEEE Transactions on 2011;17(12):2045–52.
[32] Bremer PT, Edelsbrunner H, Hamann B, Pascucci V. A multi-resolution data structure for two-dimensional morse-smale functions. In: Visualization, 2003. VIS 2003. IEEE. IEEE; 2003, p. 139–46.
[33] Edelsbrunner H, Harer J, Zomorodian A. Hierarchical morse complexes for piecewise linear 2-manifolds. 2003.
[34] Tricoche X, Scheuermann G, Hagen H. Continuous topology simplification of planar vector fields. In: Proceedings of the conference on Visualization'01. IEEE Computer Society; 2001, p. 159–66.
[35] De Leeuw W, Van Liere R. Collapsing flow topology using area metrics. In: Proceedings of the conference on Visualization'99: celebrating ten years. IEEE Computer Society Press; 1999, p. 349–54.
[36] Wang B, Rosen P, Skraba P, Bhatia H, Pascucci V. Visualizing robustness of critical points for 2d time-varying vector fields. Computer Graphics Forum 2013;32(3pt2).
[37] Leutbecher M, Palmer T. Ensemble forecasting. Journal of Computational Physics 2008;227(7):3515–39.